Accelerating the crystallization kinetics of linear polylactides by adding cyclic poly ($_L$-lactide): Nucleation, plasticization and topological effects

Marina Betegón Ruiz[1], Ricardo A. Pérez-Camargo[2*], Juan V. López[3], Evis Penott-Chang[3], Agurtzane Múgica[1], Olivier Coulembier[4], Alejandro J. Müller[1,5*]

[1]POLYMAT and Department of Polymers and Advanced Materials: Physics, Chemistry and Technology, Faculty of Chemistry, University of the Basque Country UPV/EHU, Paseo Manuel de Lardizabal 3, 20018, Donostia-San Sebastián, Spain

[2]Beijing National Laboratory for Molecular Sciences, CAS Key Laboratory of Engineering Plastics, CAS Research/Education Center for Excellence in Molecular Sciences, Institute of Chemistry, Chinese Academy of Sciences, Beijing 100190, China

[3]Grupo de Polímeros USB, Departamento de Ciencia de los Materiales, Universidad Simón Bolívar, Apartado 89000, Caracas 1080-A, Venezuela.

[4]Laboratory of Polymeric and Composite Materials, University of Mons – UMONS, Place du Parc 23, 7000 Mons, Belgium.

[5]IKERBASQUE, Basque Foundation for Science, Bilbao, Spain

*Corresponding authors: Ricardo A. Pérez-Camargo (ricardo507@iccas.ac.cn) and Alejandro J. Müller (alejandrojesus.muller@ehu.es)

For Table of Contents use Only

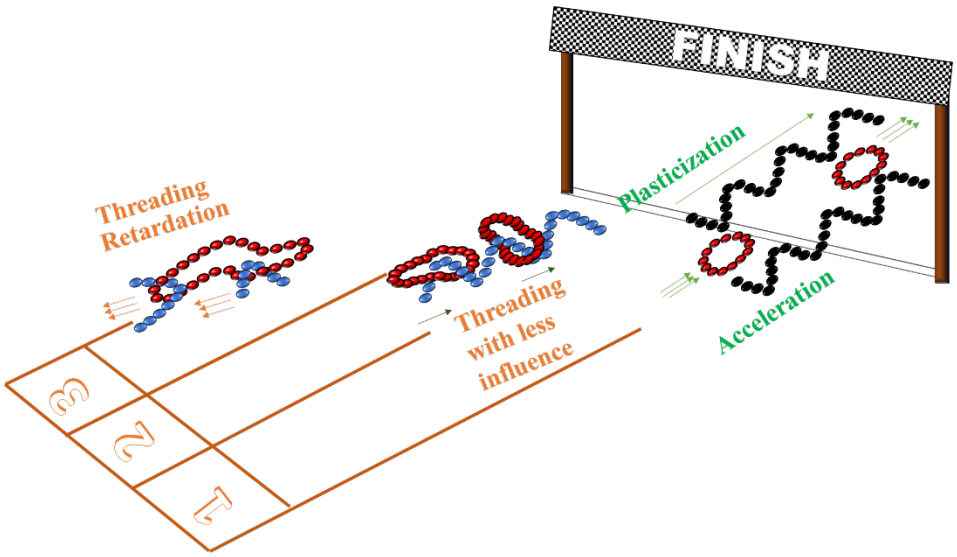

ABSTRACT

Polylactide is one of the most versatile biopolymers, but its slow crystallization limits its temperature usage range. Hence finding ways to enhance it is crucial to widen its applications. Linear and cyclic poly (L-lactide) (*l*-PLLA and *c*-PLLA) of similarly low molecular weights (MW) were synthesized by ring-opening polymerization of L-lactide, and ring-expansion methodology, respectively. Two types of blends were prepared by solution mixing: (a) *l*-PLLA / *c*-PLLA, at extreme compositions (rich in linear or in cyclic chains), and (b) blends of each of these low MW materials with a commercial high MW linear PLA. The crystallization of the different blends was evaluated by polarized light optical microscopy and differential scanning calorimetry. It was found, for the first time, that in the *l*-PLLA rich blends, small amounts of *c*-PLLA (*i.e.*, 5 and 10 wt %) increase the nucleation density, nucleation rate ($1/\tau_0$), spherulitic growth rate (G), and overall crystallization rate ($1/\tau_{50\%}$), when compared to neat *l*-PLLA, due to a synergistic effect (*i.e.*, nucleation plus plasticization). In contrast, the opposite effect was found in the *c*-PLLA rich blends. The addition of small amounts of *l*-PLLA to a matrix of *c*-PLLA chains causes a decrease in the nucleation density, $1/\tau_0$, G, and $1/\tau_{50\%}$ values, due to threading effects between cyclic and linear chains. Small amounts of *l*-PLLA and *c*-PLLA enhance the crystallization ability of a commercial high MW linear PLA without affecting its melting temperature. The *l*-PLLA only acts as a plasticizer for the PLA matrix, whereas *c*-PLLA has a synergistic effect in accelerating the crystallization of PLA that goes beyond simple plasticization. The addition of small amounts of *c*-PLLA affects not only PLA crystal growth but also its nucleation due to the unique cyclic chains topology.

Keywords: *low MW linear / cyclic PLLA blends*, *commercial high MW linear PLA, plasticization, synergistic effect, threading effect*s.

1. Introduction

Polylactide (PLA) is considered a sustainable alternative to conventional polymers (*i.e.*,

petroleum-based polymers) in different fields because, in addition to being biodegradable, it is biobased (*i.e.*, it is obtained from natural renewable sources, like sugar in corn starch and beets) and biocompatible [1]. PLA is commercially available in a wide range of grades [2], including grades for biomedical uses [3]. PLA has good oil resistance, possesses non-toxic features, and has a range of mechanical properties that have been compared to those of poly (ethylene terephthalate) (PET) [4]. All these properties allow its use in different applications, such as film and packaging (substituting conventional polymers), textile and fiber, construction, and biomedical applications, among others. Despite the advantages and potentialities of PLA, unfavorable characteristics restrict its production [5] and usage in different applications (*e.g.*, durable applications such as automotive and electronics [5]). These limitations are mainly due to the inherently low melt strength, high brittleness, slow crystallization rate, and narrow processing windows of PLA [6].

The crystallization ability and other properties of PLA depend on the ratio L- to D, L-enantiomers [7]. The presence of repeating units of different chirality reduces the crystallinity, crystallization rate, and melting point of PLA [8]. Commercially available PLA materials usually contain a mol % content of D units in the range of 1.5 to 10 %. The samples with more than 8 % mol cannot crystallize [8].

Many past studies have been devoted to increase PLA crystallization rate. The range of applications for PLA is limited by its low glass transition temperature (T_g =50 to 80 °C) [2, 4] unless crystallization can be induced to improve its thermal usage range [9]. Improving PLA crystallization implies modifying its nucleation density and its growth rate. Adding nucleating agents increases the nucleation density [10-17], whereas plasticizer addition increases chain mobility [3, 9]. The addition of both nucleating and plasticizers agents has also been reported in the literature [10]. Another alternative to improve the crystallization of PLA is blending with other

polymers [14, 18, 19].

Efficient strategies to enhance PLA crystallization must maintain its biodegradable, non-toxic, and biocompatible characters. From that point of view, the best nucleating agent and plasticizer could be based on PLA, and PLA stereocomplexes [17, 20], or even PLA with different topologies, *e.g.*, cyclic topology.

Cyclic polymers differ from their linear analogs in their lack of chain ends. This provokes unique and improved properties [21]. Different challenges remain [21, 22] related to the purity of cyclic polymers (*i.e.*, quantification and identification of non-cyclic impurities), purification methods, and scalability [21, 22], but significant advances have been performed in their preparation methods [21-23]. Several potential applications (especially biomedical ones) are recognized, as reported in recent reviews [21, 22, 24]. The unique cyclic topology seems to be suitable for some biomedical applications. Compared to linear analogs, cyclic polymers exhibit large blood circulation times (improving targeting tumors) [21, 22] and possess higher transfection (gene transfection) efficiency than the linear ones [21]. In the micelle-based drug delivery, the cyclic polymers and copolymers can tune the micelle size and stability due to their self-assembly characteristics [21,22]. Thus, cyclic polymers can have a crucial role in the advancement of the fields mentioned above.

From the crystallization point of view, the comparisons of cyclic and linear polymers in the literature show different and sometimes even opposite trends [1, 25-44], hence, their crystallization is still a debated topic [22]. As an alternative for such debate, simulations studies have been performed, but even for them, contradicting results have also been found in their predictions of the relative melting and equilibrium melting temperatures of cyclic and linear polymers [45-47]. However, most studies, both experimental and simulated, employing cyclic and linear polymers,

have shown that cyclic polymers exhibit enhanced nucleation [28, 29, 43], faster spherulitic growth rates (*G*) [30-33, 44] and faster overall crystallization [25, 26, 34-42] (as determined by DSC, which includes both nucleation and growth) compared to their linear counterparts. Therefore, employing cyclic polymers as an additive to enhance the crystallization of linear PLA seems to be a good strategy.

The research related to cyclic and linear polymer blends is scarce, and in most of the cases, has been focused on molecular dynamic simulations [46, 48-54] and diffusion studies [55], in which, ring and linear chain sizes are important factors. Shin et al. [56] blended cyclic and linear PLLA and PDLA to study stereocomplexation. It has been recognized that small amounts of linear chains dramatically affect the properties of the cyclic polymers due to threading effects. Threading refers to the action of linear chains that can reptate and thread through cyclic chains, thereby joining several chains together thus affecting diffusion and relaxation times. Threading effects have been reported by Kapnistos et al. [57], López et al. [36], and Pérez et al. [35] in cyclic/linear polystyrene (PS) blends, cyclic/linear poly (ε-caprolactone) (PCL) blends, and cyclic/multi-walled carbon nanotubes-*grafted*-linear-PCL (MWCNT-*g*-*l*-PCL) nanocomposites, respectively.

In the work of López et al. [36], it was found that small amounts of linear PCL cause a deviation with respect to a simple mixing law. Only when the linear PCL content is increased, the experimental points follow a linear mixing law. However, the influence of small amounts of cyclic PCL on a linear PCL matrix has not been investigated yet. The different works of cyclic/linear blends focus on adding small amounts of linear polymer to a cyclic matrix. None of these works have explored the opposite case, leaving pending questions: What happens when small amounts of cyclic chains are added to a linear matrix? Is the threading effect still present? Are molecular weight differences between linear and cyclic chains relevant for the blends behavior?

In the present work, we will answer these questions by studying linear/cyclic PLLA blends, which maintain the exceptional characteristics of the PLA, in a composition range where small amounts of cyclic chains are added to a matrix of linear chains and *vice-versa*. As far as the authors are aware, this is the first time that both composition ranges (*i.e.*, linear rich and cyclic rich blends) have been explored. We will also investigate for the first time, the topological influence of low MW linear and cyclic PLLAs as additives for a commercial PLA (with high MW), and thus design fully biobased, biodegradable, and biocompatible thermoplastic blends. We show that chain topology can have dramatic effects on the nucleation and crystallization rates of linear/cyclic PLA blends.

2. Experimental Part

2.1. Materials

The cyclic PLLA (*c*-PLLA) used in this work was synthesized by ring-expansion. According to Matrix-Assisted Laser Desorption/Ionization-Time of Flight (MALDI-TOF) mass spectrometry experiments, there are 98% of *c*-PLLA chains in the sample, with a number average molecular weight (M_n), M_n=9.0 kg/mol. The cyclic nature of the *c*-PLLA was proved by confronting the experimental MS chromatogram (MALDI-TOF analysis) to an isotopic model (see Figure S1). Furthermore, Size Exclusion Chromatography (SEC) analysis were performed, obtainingM_n = 13.5 kg/mol, dispersity index of 1.33, and the absent of significant linear traces (see Figure S2).An analogous linear PLLA (*l*-PLLA) was synthesized by ring-opening polymerization of L-lactide, obtaining a *l*-PLLA with a M_n=15.5 kg/mol and a dispersity index of 1.5. Both *c*- and *l*-PLLA were obtain from 100% $_L$-lactide monomers with a controlled synthetic procedure that avoids racemization [58-59]. Details on the methods used to produce cyclic and linear PLAs are reported in ref. [58] and [59], respectively.

Table 1. List of prepared blends.

Material	**PLA content (wt %)**	***l*-PLLA content (wt %)**	***c*-PLLA content (wt %)**
l-PLLA	-	100	-
c-PLLA	-	-	100
PLA	100	-	-
l-PLLA / *c*-PLLA 95/5	-	95	5
l-PLLA / *c*-PLLA 90/10	-	90	10
l-PLLA / *c*-PLLA 5/95	-	5	95
PLA / *l*-PLLA 95/5	95	5	-
PLA / *c*-PLLA 95/5	95	-	5

Linear/Cyclic (*l*-PLLA/*c*-PLLA) blends were prepared in solution, using chloroform, $CHCl_3$, as a solvent. In all the cases, 4 mg of solid material were dissolved in 1 mL of $CHCl_3$. Small amounts, 5 and 10 wt %, of *c*-PLLA (*i.e.*, around 0.2 mg) were added in a *l*-PLLA matrix (*i.e.*, around 3.8 mg) and *vice-versa*. The mixture was placed directly in DSC pans, dried in a vacuum oven (to avoid any solvent), at 60 °C, until obtaining a constant weight (this process can take several hours). The prepared blends are shown in Table 1.

A commercial high molecular weight (MW) linear PLA, synthesized by ring-opening polymerization of lactide, was provided by NatureWorks (commercial name 4032D). This PLA

has a $_D$-lactide content of 2% mol, an M_n=123 kg/mol, and a dispersity index of 1.72. The PLA was blended (*i.e.*, following the procedure described above), in solution, with 5 wt % of *c*- or *l*-PLLA, as is indicated in Table 1.

2.2. Polarized light optical microscopy (PLOM) experiments: Crystallization from the melt state

Morphological observations, as well as nucleation density, and spherulitic growth rate experiments were performed by filming spherulites growing in an Olympus BX51 PLOM, equipped with a λ plate (*i.e.*, a red tint plate) between the polarizers at 45°. The samples were prepared by solving-casting, with 1.3 % of the weight of the materials dissolved in $CHCl_3$. One drop of this solution was placed in a glass cover, and then the solvent was evaporated. The samples were heated in a temperature-controlled hot stage (Mettler FP82HT). The thermal history of the samples was erased at 190 °C for 3 minutes, and then the samples were cooled at 50 °C/min until the desired crystallization temperature (T_c). In the case of nucleation density experiments, a constant T_c and a constant crystallization time were selected for comparison purposes. For spherulitic growth rate experiments, we selected T_c in a range of 105 to 130 °C, with intervals of 5 °C.

2.3. Non-isothermal differential scanning calorimetry (DSC) experiments

Standard non-isothermal DSC tests, as well as isothermal tests, were performed in a Pyris 1 DSC of PerkinElmer with an Intracooler 2P as a cooling device. The DSC was operated with an ultrapure N_2 atmosphere, maintaining a constant flow of 20 mL/min, and it was calibrated with indium and tin standards. For the standard non-isothermal test, as received samples were encapsulated in aluminum DSC pans and heated at 10 °C/min, until 190 °C. Their thermal history

was erased by holding at 190 °C for 3 minutes. Subsequently, the samples were cooled, at 5 or 20 °C/min, until 0 °C, registering the crystallization (*i.e.*, in those cases in which it occurred). A holding step, of 1 minute, at 0 °C, was used. Then a heating scan, at 20 °C/min was performed to register the different thermal transitions.

2.4. Isothermal DSC experiments: Crystallization from the glassy state

The isothermal crystallization of the PLA samples employed in this work was too slow to follow them from the melt state. In order to increase the overall crystallization rate, the samples were first cooled from the melt to a temperature below the glass transition temperature, T_g, to allow for vitrification and nucleation during cooling. Then, the sample was quickly heated from the glassy state up to the selected T_c value, where the crystallization was followed by isothermally recording the heat evolved as a function of time with the DSC. The following steps were applied to the samples:

a. Erase of the thermal history at 190 °C for 3 minutes.
b. Cooling from 190 °C to 0 °C, at 60 °C/min. Note that the temperature of 0 °C is below T_g of the PLA, which is around 60 °C.
c. Hold the sample at 0 °C for 1 minute.
d. Heat the sample from 0 °C to the selected T_c (a range of 85 to 130 °C, with increments of 5 °C was employed), at 60 °C/min (a rate at which no crystallization can occur during heating).
e. Hold the sample at T_c enough time to complete its crystallization under isothermal conditions. Often, a time of 30 minutes was enough to complete the crystallization process.
f. Heat the sample from T_c to 190 °C at 20 °C/min to register the heating behavior after the isothermal crystallization.

3. Results and Discussion

In this work, we have evaluated the behavior of two different kinds of blends:

(a) low MW *l*-PLLA with small amounts of *c*-PLLA and *vice-versa* (Section 3.1) and

(b) commercial high MW linear PLA with small amounts of low MW *l*-PLLA or *c*-PLLA (Section 3.2).

The different effects generated in these blends are discussed below.

3.1. Topological effect in cyclic and linear low MW PLLA blends

In this section, the blends of *l*-PLLA with small amounts of *c*-PLLA, and mirror compositions (*i.e.*, *c*-PLLA with small amounts of *l*-PLLA, see compositions in Table 1) are analyzed with different techniques.

3.1.1. Polarized Light Optical Microscopy results: Isothermal crystallization from the melt state.

Figure 1 shows the spherulitic morphology (*i.e.*, negative spherulites for the neat materials and their blends) obtained after the samples were crystallized from the melt at a T_c=115 °C for 10 minutes for both *l*-PLLA, *c*-PLLA and their blends.

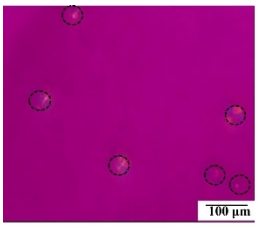

(a) *l*-PLLA

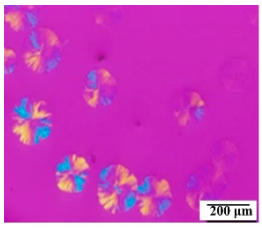

(b) *l*-PLLA/ *c*-PLLA 95/5

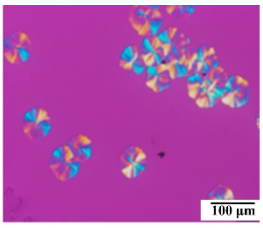

(c) *l*-PLLA/ *c*-PLLA 90/10

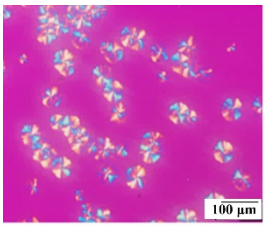

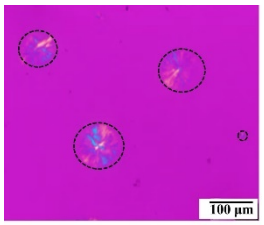

(d) *c*-PLLA (e) *l*-PLLA/ *c*-PLLA 5/95

Figure 1. PLOM micrographs taken after crystallization from the melt of the samples at 115 °C for 10 minutes. Circles are used in 1a and 1e to indicate the spherulites present in the micrographs.

By using the same conditions of isothermal crystallization temperature (T_c=115 ºC) and time (10 min), it is possible to compare qualitatively the nucleation density in Figure 1, and analyze the different effects caused by the addition of cyclic and linear PLLA in the blends.

Nucleation: Threading vs. nucleation effect

Figures 1a and 1d show that *c*-PLLA has a much higher nucleation density than its linear analog (i.e., *l*-PLLA). This is in line with the results reported in the literature for *l*-PLLA and *c*-PLLA and PDLA [27], of slightly higher MW (~14 kg/mol (*c*-PLLA) and 16.7 kg/mol (*l*-PLLA)), and other linear and cyclic polymers, such as polyethylene (PE) [29], PTHF [28, 43], and PCL [25, 34]. The differences in nucleation have been attributed to the cyclic topology (note that the MWs of the *l*-and *c*-PLLA employed in this work are similar) since it is characterized by a lack of chain ends and more collapsed coil conformations in the melt. Therefore, it is expected that cyclic chains nucleate faster than linear chains of similar MWs [25, 26].

Figures 1b and 1c show that as the *c*-PLLA content increases in the *l*-PLLA/ *c*-PLLA blends (*i.e.*, from 5 to 10 wt %), the number of nuclei increases. Thus, the small amount of *c*-PLLA acts as a nucleating agent of the *l*-PLLA, despite the fact that their presence might lead to threading events with the linear chains. It has been reported that small amounts of cyclic chains do not affect

the overall conformation and dynamics of the linear chains [50]. The reason for this behavior is that a large fraction of linear chains do not experience any interactions with cyclic chains [50].

In contrast, adding small amounts of *l*-PLLA to the *c*-PLLA matrix generated the opposite effect. Figure 1e shows that small amounts of *l*-PLLA lead to a reduction in the number of nuclei of the *l*-PLLA/*c*-PLLA 5/95 blend. Thus, the small amounts of *l*-PLLA act as an anti-nucleating agent of the *c*-PLLA as these linear chains thread through the cyclic ones, creating extra entanglement points that hinder the nucleation and diffusion of cyclic chains (see the illustration in Scheme 1b and its discussion below). This chain threading effect has been reported before for cyclic/linear PS and PCL blends by López et al. [36] and Kapnistos et al. [57], respectively, and for cyclic/MWCNT-*g*-*l*-PCL blends by Pérez et al. [35].

Spherulitic growth kinetics: Plasticization vs. threading effects

By measuring the growth of the spherulites by PLOM in a wide T_c range, we have evaluated the influence of blending linear and cyclic chains on spherulitic growth (G) kinetics. Figure 2 shows the G values (i.e., spherulitic growth rates) vs. T_c for all the materials examined in this work.

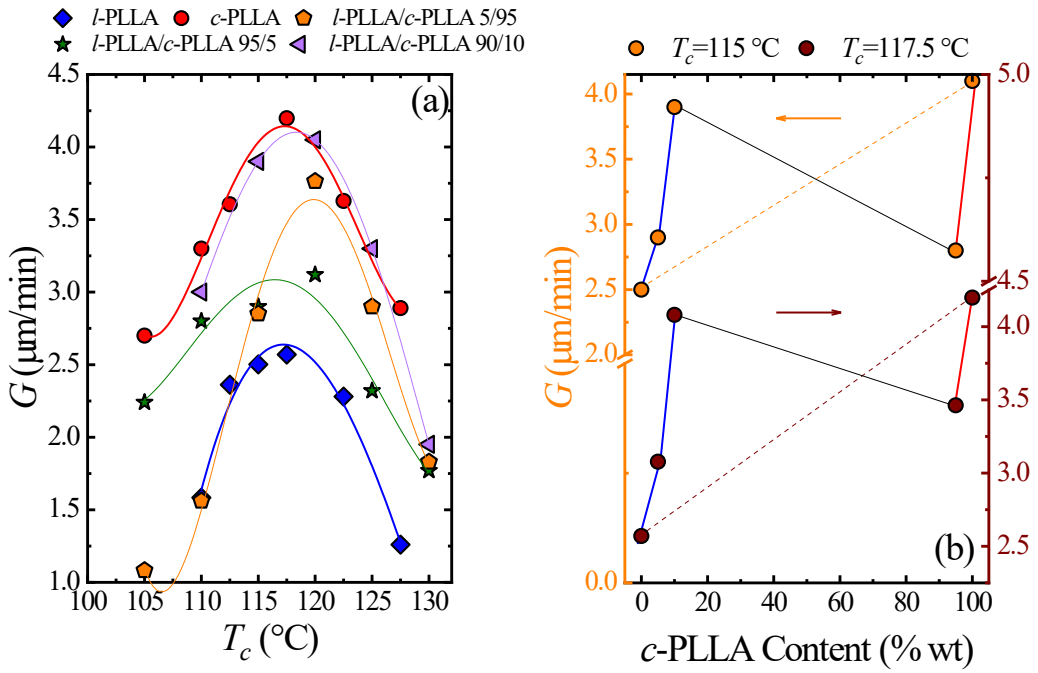

Figure 2. (a) Spherulitic growth rate (G) as a function of the crystallization temperature (T_c) for *l*-PLLA, *c*-PLLA and their blends (solid lines are used to guide the eye), and (b) G vs. *c*-PLLA content at constant selected T_c=115 °C and 117.5 °C. The dashed lines represent linear mixing laws, the solid lines (blue and red) are used to guide the eye.

Figure 2a shows the typical bell-shape behavior of the G vs. T_c curves caused by the competition between secondary nucleation (high temperatures or low supercoolings) and diffusion (low temperatures or high supercoolings) [27]. By comparing the G vs. T_c curves of the *l*-PLLA and *c*-PLLA, it is obvious that significantly higher G values are obtained for *c*-PLLA. Such difference (also reflected on energetic parameters obtained by fits to the Lauritzen and Hoffman theory, as shown in Table S7) is caused by the faster diffusion rate at high supercoolings (*i.e.*, related to compact coil conformation, lower entanglement density, and enhanced supercooling degree [36]) of the cyclic chains in comparison to linear ones [26, 44]. Yamazaki et al. [44] determined that the term proportional to the diffusion constant, G_0 [60, 61], is higher for cyclic PCLs than for linear analogs in a wide range of MW. In the present work, our results suggest that

in the low supercooling temperature range (right hand side of the bell shape curve in Figure 2a), the increase in *G* values for PLLA cyclic chains is due to the higher secondary nucleation rate of the ring like chains in comparison with linear ones.

Sample purity can affect the results of spherulitic growth rate. Zaldua et al. [27] reported similar *G* values for *l*- and *c*-PLLA. The results were explained by the presence of a small fraction of linear or higher MW cycles detected by SEC. Such impurities retard spherulitic growth rates of *c*-PLLA, in such a way that they can be comparable to those of *l*-PLLA. Hence, the higher difference between $G_{c\text{-}PLLA}$, and $G_{l\text{-}PLLA}$ found here (Figure 2a) is probably related to a small amount of linear impurities in the samples used in the present work.

For clarity, we plotted *G* values measured at constant T_c (for two temperatures, T_c=115 °C, and 117.5 °C) versus *c*-PLLA content in Figure 2b. As *c*-PLLA is added to *l*-PLLA, a remarkable increase in *G* values is observed. When 10 wt % of *c*-PLLA is added, the *G* value of the *l*-PLLA/ *c*-PLLA 90/10 blend is comparable to the value for neat *c*-PLLA. Thus, small amounts of *c*-PLLA cause a plasticization-like effect on the *l*-PLLA matrix, explaining the increase in *G* values observed (see Scheme 1a). An acceleration of the diffusion of linear chains in the presence of rings was predicted by Subramanian and Shanbhag [53], who studied symmetric and asymmetric cyclic / linear blends of polymers by simulations. However, this had never been corroborated experimentally until now, thanks to the results presented here. They have also reported that in some cases, the linear chains remain practically unaffected by the ring ones, whereas, as expected, ring chains always show slower diffusion in the blends [50].

An opposite effect is obtained when *l*-PLLA is added to *c*-PLLA. This behavior is explained by the threading effect of small amounts of *l*-PLLA on *c*-PLLA, which hinders both secondary nucleation and diffusion of cyclic molecules (see Scheme 1b). This trend corroborates

the findings of previous works [35, 36]. Figure 2b also shows a solid black line (representing the mixing law) indicating that both, plasticization-like effects and threading effects will be diluted as the *c*-PLLA or *l*-PLLA content increases, and hence, the mixing law will be recovered, as were found in cyclic/linear PCL blends [36]. The differences as T_c increases (115 °C vs. 117.5 °C), in Figure 2b, are related to the decrease of the melt viscosity, which reduces the effect of diffusion [36].

3.1.2. DSC Non-isothermal experiments

Figure 3a shows the DSC second heating (at 20 ºC/min) for *l*-PLLA, *c*-PLLA and their blends, after they were previously cooled from the melt (at 5 °C/min) (see Figure S3). The different transitions obtained from these scans are listed in Tables S1 and S2 of the SI.

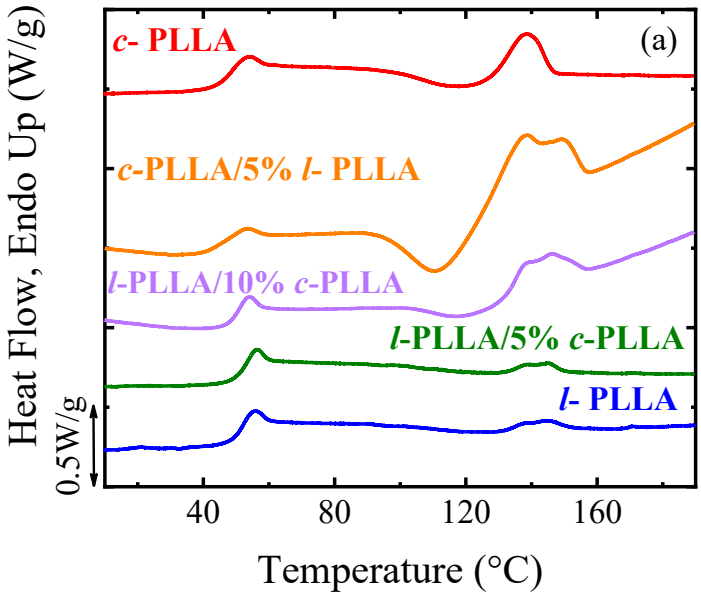

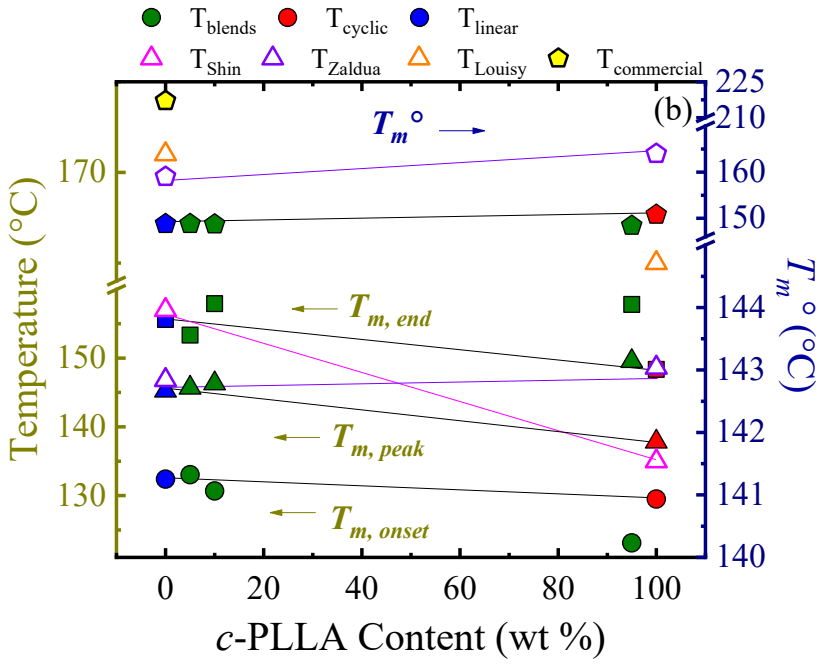

Figure 3. (a) Second heating DSC scans, at 20 °C/min, after a previous cooling from the melt at 5 °C/min, for *l*-PLLA, *c*-PLLA and their blends. (b) A comparison of $T_{m,\ onset}$, $T_{m,peak}$, and $T_{m,end}$ values obtained from Figure 3a (for *l*-PLLA (T_{linear}), *c*-PLLA (T_{cyclic}), and their blends (T_{blends})) with values reported in the literature, as a function of the *c*-PLLA content. The values of the equilibrium melting temperature ($T_m°$) obtained in this work, including the commercial PLA ($T_{commercial}$), are reported, together with the T_m values of the literature: T_{Shin} [56], and T_{Louisy} [1]; and the T_m and $T_m°$ reported by Zaldua et al. [27] (T_{Zaldua}). Note that the T_m values obtained by Louisy et al. [1] are comparable to the $T_m°$.

Figure 3a shows first the characteristic endothermic step due to the T_g of the materials, in line with the one registered during the cooling scans (see Figure S3). The T_g is followed by a broad cold-crystallization peak (T_{cc}). The T_g values, in this case, do not vary significantly between neat cyclic and linear chains, and neither when *c*-PLLA is added to the *l*-PLLA matrix. However, the opposite (*i.e.*, adding *l*-PLLA to the *c*-PLLA matrix) causes an increase in T_g due to the diffusion difficulties of the threaded cyclic chains by the linear ones.

The position of the T_{cc} is generally correlated to the nucleation, *e.g.*, the lower the value of T_{cc}, the larger the nucleation density. Although the T_{cc}-nucleation qualitative relationship might be difficult to establish, as T_{cc} values are obtained during non-isothermal experiments, it can still be

used to illustrate some trends. In this work, the T_{cc} position reflects the higher nucleation ability of the *c*-PLLA, since the $T_{cc,\ c\text{-}PLLA}$ (117 °C) < $T_{cc,\ l\text{-}PLLA}$ (121 °C). Zaldua et al. [27] found similar trends (compared to this work), *i.e.*, lower T_{cc} for *c*-PLLA and *c*-PDLA than *l*-PLLA and *l*-PDLA, and the results were consistent with their nucleation measurements by PLOM. They attributed the differences in the T_{cc} values and nucleation density to the larger supercooling and the more compact coil conformations of the cyclic chains [26, 27]. They discarded any structural influence since the X-rays characterization showed the same crystal structure for both cyclic and linear PLLA and PDLA [27].

The values of $T_{m,onset}$, $T_{m,peak}$, and $T_{m,end}$ values for *l*-PLLA, *c*-PLLA and their blends extracted from Figure 3a are shown in Figure 3b as a function of composition. In the particular case of *l*-PLLA and *c*-PLLA, all values reported in the literature have also been plotted for comparison purposes. Figure 3b shows that the melting point values for *l*-PLLA are slightly larger than those of *c*-PLLA in agreement with values reported in the literature by Louisy et al. [1] and Shin et al. [56]. Zaldua et al. [27], on the other hand, found slightly higher values for $T_{m,c\text{-}PLLA}$ (148.6 °C) in comparison with $T_{m,l\text{-}PLLA}$ (146.8 °C). Higher T_m values of linear polymers with respect to its cyclic counterparts have also been reported for other linear and cyclic polymers [26]. Such a trend has been attributed to higher melting entropies of the cyclic polymers in comparison with the linear ones [28, 43]. However, other factors should be considered, as the differences in T_m values could be influenced by:

(1) differences in the synthetic methods (*i.e.*, ring closure click chemistry [27] vs. ring expansion (in this work), zwitterionic ring-opening polymerization [56], and reactive extrusion [1]),

(2) differences in MWs (*i.e.*, 13 kg/mol (in this work), and 15, 16, and 29 kg/mol in the

works of Shin et al. [56], Zaldua et al. [27], and Louisy et al. [1], respectively). Note that in Figure 3b, the highest value of the equilibrium melting temperature, $T_m°$ (*i.e.*, 217 ºC) is that detected for the commercial linear PLA with has a much higher MW than any of the other samples.

(3) the critical issue of purity of the cyclic chains, which always contain even a very small amount of linear chains.

In this work, we also determined the $T_m°$ for *l*-PLLA, *c*-PLLA and their blends (see Table S5 on the SI). Remarkably, Figure 3b shows that $T_{m,\,c\text{-}PLLA}^{o} > T_{m,\,l\text{-}PLLA}^{o}$ and that the trend with composition is a straight line consistent with a simple linear mixing law, except for the *l*-PLLA / *c*-PLLA 5/95 blend, where the threading effects produced a melting point depression. Please note that Zaldua et al. [27] also reported a similar trend with $T_{m,\,c\text{-}PLLA}^{o} > T_{m,\,l\text{-}PLLA}^{o}$. This is an interesting result considering that in other cyclic polyesters, like PCL, it has also been reported that the $T_m°$ of the cyclic chains is higher than their linear analogs [26, 44]. Müller et al. [26, 34] have argued that cyclic polymers have a lower melt configurational entropy than the linear ones, assuming that in the crystalline state, the entropy is the same in both cases [26]. In this work, the apparent (kinetic) melting points determined by non-isothermal crystallization of the linear chains seem to be slightly higher than those of the cyclic PLLA chains, whereas the apparent melting points determined after isothermal crystallization (see Figure S7 on SI) show the opposite trend (*i.e.*, most values of *c*-PLLA are higher than *l*-PLLA) instead. This result is consistent with the trends obtained for the $T_m°$.

Figure 3a shows that as the *c*-PLLA content increases in the blends, the T_{cc} values decrease compared to that of *l*-PLLA, indicating an increase in the nucleation density. In the *l*-PLLA addition to the *c*-PLLA matrix, the expected T_{cc}-nucleation density qualitative relationship is not observed since the *l*-PLLA / c-PLLA 5/95 shows a slightly lower T_{cc} than that of *c*-PLLA. As we

mentioned before, the T_{cc} determination is made from non-isothermal tests, and in some cases, this can generate deviations concerning the expected behavior. The nucleation results obtained from the glassy state during the second heating DSC scans in non-isothermal conditions (except for the *l*-PLLA / *c*-PLLA 5/95) are nevertheless consistent with the PLOM observations that also show similar differences in nucleation density during isothermal crystallization from the melt.

The results obtained by DSC and PLOM show that adding small amounts of *c*-PLLA to a linear PLLA matrix increases both the nucleation density (Figures 1 and 3) and the spherulitic growth rates (Figure 2). In contrast, the opposite effect is obtained (by PLOM) by adding small amounts of *l*-PLLA in the cyclic PLLA matrix.

3.1.3. Overall isothermal crystallization: Crystallization from the glassy state.

Isothermal DSC measurements follow the complete solidification of the material, including nucleation and growth from the glassy state. The time elapsed before any exothermic heat, can be recorded in the DSC experiment at a constant T_c value, is known as the induction or incubation time (τ_0). The inverse of the incubation time ($1/\tau_0$) can be considered the primary nucleation rate before any growth starts.

Figure 4 shows the $1/\tau_0$ and the experimental overall crystallization rate from the glassy state (expressed as the inverse of the half-crystallization time, *i.e.*, $1/\tau_{50\%}$) as a function of T_c for *l*-PLLA, *c*-PLLA, and their blends.

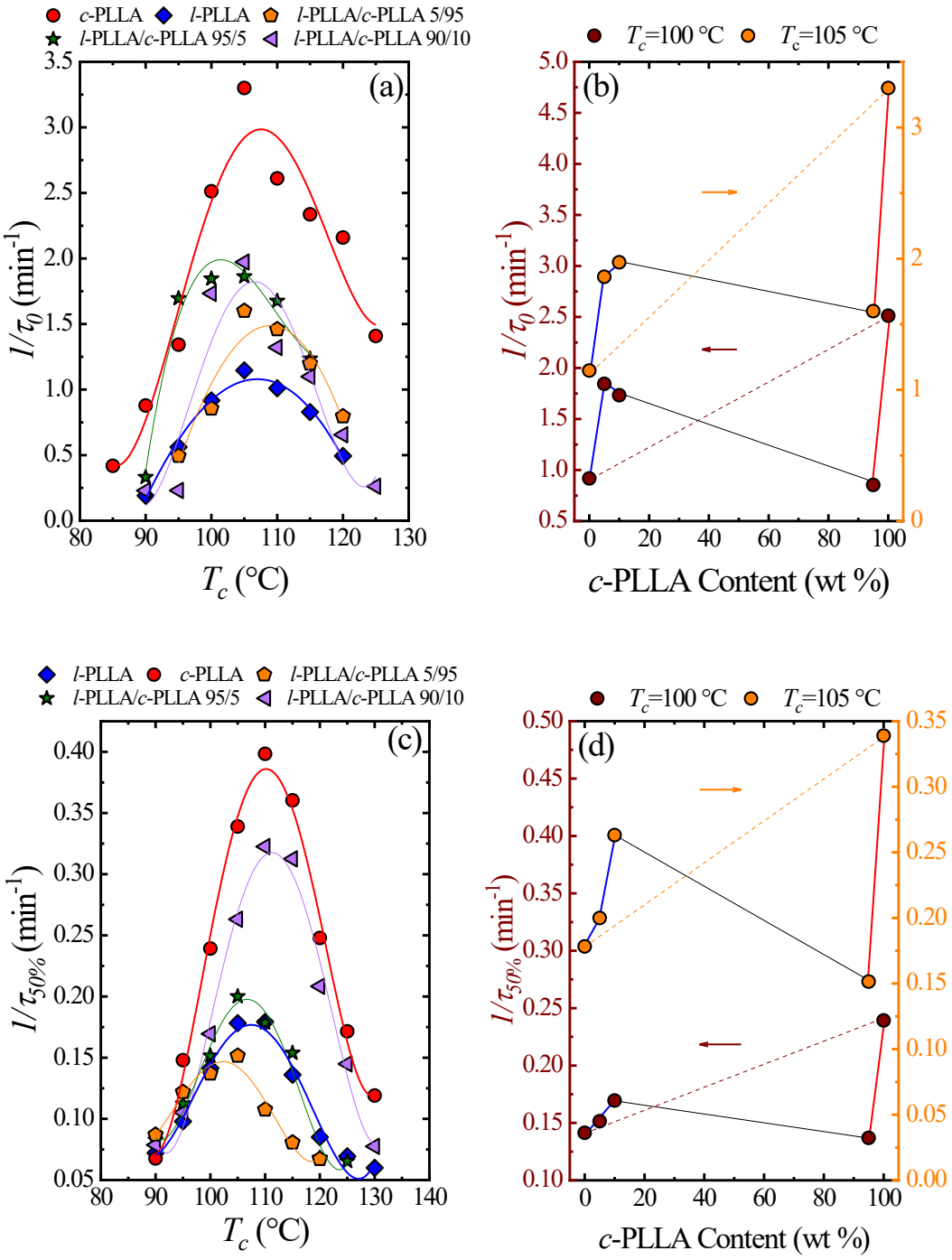

Figure 4. (a) $1/\tau_0$ and (c) $1/\tau_{50\%}$ as a function of T_c for *l*-PLLA, *c*-PLLA and their blends (we employed solid lines to guide the eye), and (b) $1/\tau_0$ (T_c=100 °C and 105 °C) and (d) $1/\tau_{50\%}$ (T_c=100 °C and 105 °C) as a function of *c*-PLLA content. The dashed line in (b) and (d) indicates a simple mixing law, and the solid black line indicates the expected recovery of the mixing law.

Figure 4a and Figure 4c show that *c*-PLLA has a faster nucleation rate ($1/\tau_0$) and faster overall crystallization kinetics ($1/\tau_{50\%}$) from the glassy state, respectively, than *l*-PLLA in a broad T_c range. These results are in line with the nucleation and spherulitic growth rate PLOM results (from the melt state) presented above and with literature results for cyclic and linear PLLA and PDLA [27]. The isothermal conditions can be considered more suitable to determine $1/\tau_0$-nucleation density qualitative relationships than non-isothermal T_{cc} values.

As *c*-PLLA content in the blends increases, both $1/\tau_0$ and $1/\tau_{50\%}$ values increase. A synergistic effect explains such increases. On one hand, the addition of *c*-PLLA accelerates the nucleation of the *l*-PLLA matrix, thereby acting as a nucleating agent. On the other hand, the *c*-PLLA also enhances the spherulitic growth rate of the *l*-PLLA matrix (at high supercoolings) since *c*-PLLA acts like a plasticizer. Despite the similar MWs, *c*-PLLA has a faster molecular diffusion due to its compact coil conformation without chain ends, see Scheme 1a. In the low supercooling range, the secondary nucleation is also facilitated by cyclic chains addition.

In contrast, adding small amounts of *l*-PLLA to a *c*-PLLA matrix causes a decrease of both $1/\tau_0$ and $1/\tau_{50\%}$ because of the threading effect of linear chains through cyclic chains, see Scheme 1b. The threading effect decreases nucleation (both primary and secondary nucleation) and diffusion. The differences in diffusion and in the effectiveness of the threading effects are illustrated in the cartoons presented in Scheme 1. It is important to note that the threading effect is only effective when a small number of linear chains are added to the cyclic chains, as any given linear chain can entangle with several cyclic chains. Conversely, adding *c*-PLLA to a matrix of linear chains will produce some threading effects, which can be offset by their plasticizing action, which enhances diffusion (see Scheme 1).

To better analyze the effects produced by the addition of linear and cyclic PLLA to the

cyclic and linear matrices, we have plotted, in Figures 4b and 4d, the $1/\tau_0$ and $1/\tau_{50\%}$ values obtained at a constant T_c, as a function of the *c*-PLLA content. In Figures 4b and 4d, we have drawn a dashed line that joins the neat *l*-PLLA and *c*-PLLA experimental points to represent the expected results from a mixing law. As T_c increases (to low supercoolings) a decrease in the diffusion control is expected, resulting in $1/\tau_{50\%}$ values closer to the expectations of the mixing law [36].

From Figures 4b and 4d, it is clear that either adding *c*-PLLA or *l*-PLLA to the blends causes a strong deviation from the mixing law. For *l*-PLLA-rich blends, the deviation is positive (*i.e.*, enhanced properties compared to the behavior predicted bya simple mixing law), indicating a synergistic effect obtained by adding 5 or 10 wt % of *c*-PLLA, especially for the later one. In contrast, for the *c*-PLLA-rich blends, the deviation is negative (*i.e.*, reduced properties compared to the behavior predicted by a simple mixing law) as a result of the threading effects.

As far as the authors are aware, this is the first time that synergistic and antagonistic effects in the extremes of cyclic / linear PLLA blends and cyclic / linear polymers are obtained, offering the complete picture regarding the crystallization behavior of cyclic / linear blends. Both effects are schematically illustrated in Scheme 1, as explained above.

Understanding the plasticization-like and threading effects

Scheme 1a shows that in the *l*-PLLA-rich blends, the addition of *c*-PLLA accelerates *l*-PLLA chain diffusion due to a plasticization-like effect (produced by the peculiar topology of cyclic chainswith compact coil conformations). Even though some threaded chains might be present (see the bottom part of Scheme 1a), the much larger fraction of unthreaded chains determine the properties of these blends.

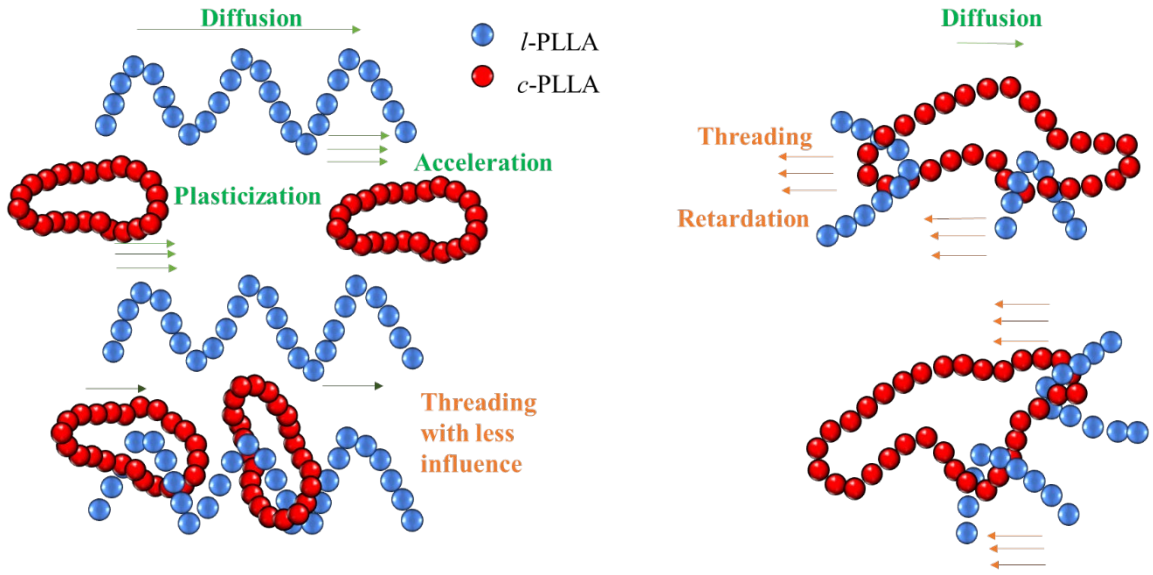

(a) *l*-PLLA-rich blend (b) *c*-PLLA-rich blend

Scheme 1. Schematic representation of different effects on chain diffusion in blends rich in (a) *l*-PLLA, and (b) *c*-PLLA.

In Scheme 1b, the threading effect of *c*-PLLA by *l*-PLLA chains in *c*-PLLA-rich blends is shown. In this case, the threading effect slows down the diffusion of cyclic chains, and we can consider that linear chains thread most of the cyclic ones. We can assume that a cyclic chain is equivalent to two covalently connected linear chains; therefore, each threaded chain will affect two chains (instead of one, as in a linear matrix). Also, it has been found, with simulations, that one linear chain can thread more than one cyclic molecule [50]. Therefore, the threading effect of the linear chains on the ring molecules has a larger influence when the matrix of the blend in made up of cyclic chains than in the opposite case.

Further analysis of the overall crystallization behavior from the glassy state was performed by using the Avrami [62, 63] and the Lauritzen and Hoffman [64, 65] (LH) theories (see details on Sections S4 and S6 of the SI).

Avrami and Lauritzen and Hoffman Theories: Threading vs. Synergistic effect

The Avrami index (n) and the constant proportional to the overall crystallization rate (K) were obtained [62]. The obtained n values, in some cases are low (see Table S4 on the SI) as the isothermal crystallization was performed from the glassy state, enhancing the nucleation density [27]. However, they can be approximated to $n = 3$, in many cases, indicating that instantaneously nucleated 3D spherulites have been obtained. The n values do not show specific trends regarding the topology. The K values (expressed in min^{-n}) were transformed to $K^{1/n}$ (expressed in min^{-1}) for comparison purposes. The $K^{1/n}$ vs. T_c curves follow the same trend as the $1/\tau_{50\%}$, indicating the goodness of the fit (see Figure S6). For more details, see Section S4 on the SI.

From the heating DSC traces, after the isothermal crystallization experiments, we have determined the $T_m°$ using the Hoffman-Weeks (HW) extrapolation (See Section S5 on the SI). We found that $T_m°_{,c\text{-}PLLA} > T_m°_{,l\text{-}PLLA}$ (150.8 vs. 148.8 °C), which is in line with previous studies on PLAs [27], as well as on other cyclic and linear polymers [26] (*e.g.*, PCL [34, 44]), even in a wide range of MWs [44]. When small amounts of *c*-PLLA are added to the *l*-PLLA matrix, the $T_m°$ remains within a linear simple mixing law line (see Figure 3b). In contrast, due to threading effects, small amounts of *l*-PLLA cause a $T_m°_{,c\text{-}PLLA}$ depression (*i.e.*, from 150.8 °C to 148.4 °C) in the *l*-PLLA/*c*-PLLA 5/95 blend.

The LH theory allows us to quantify energetic parameters related to the crystallization process. Applying the LH theory with the Origin plug in developed by Lorenzo et al. [62], (now converted into an Origin App, see ref. [66]), we have obtained the K_g^{τ} values, using for its calculation the $T_m°$ values obtained by the HW extrapolation and the parameters indicated in Section S6 of the SI. The K_g^{τ} is a parameter proportional to the energy barrier that the polymer needs to overcome for the overall crystallization (as it is obtained by isothermal DSC studies,

which include both nucleation and growth). The obtained K_g^{τ} values are plotted in Figure 5 for *l*-PLLA, *c*-PLLA and their blends. It is worth noting that the obtained values are lower than those reported in the literature because of the low MW of the samples; for more details, see reference [8].

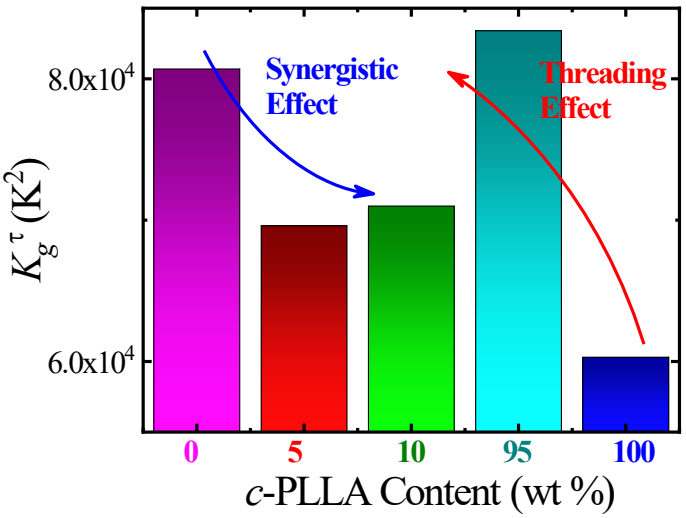

Figure 5. K_g^{τ} values as a function of the *c*-PLLA content for for *l*-PLLA, *c*-PLLA and their blends. The arrows indicate the influence of the different effects (synergistic effect and threading effect) on the K_g^{τ} values.

Figure 5 shows that the K_g^{τ} value for *c*-PLLA is lower (indicating a lower energy barrier for overall crystallization) than that for *l*-PLLA because of the topological differences between the samples. The addition of *c*-PLLA to a *l*-PLLA matrix causes a decrease in the K_g^{τ} value, attributed to a synergistic effect. Such synergistic effect is due to the dual action of cyclic chain addition: nucleation plus plasticization effects. In contrast, the addition of *l*-PLLA to a *c*-PLLA matrix increases the K_g^{τ} to values that are even higher than that of neat *l*-PLLA, evidencing the strong influence of the threading effect when small amounts of *l*-PLLA are added to a matrix of cyclic chains. Table S7 on the SI shows that K_g^{G} (growth only) values (obtained from PLOM data), are

lower than K_g^{τ} (nucleation plus growth) values (obtained from DSC data), as expected [67, 68].

3.2. Plasticization of *l*-PLLA and *c*-PLLA on commercial hign MW PLA: Role of topology.

Small amounts of *l*-PLLA and *c*-PLLA of low MWs (*i.e.*, the same materials employed in the previous section), were blended with a commercial PLA (*i.e.*, with a much higher MW). The addition of low MW PLLA chains is expected to cause a plasticization effect of the commercial PLA sample employed. But, will there be any influence of chain topology? In this section, we answer this question by analyzing, for the first time, the effect of *l*-PLLA and *c*-PLLA addition on the crystallization of a commercial PLA matrix.

3.2.1 Polarized Light Optical Microscopy (PLOM) results: Crystallization from the melt state.

Figure 6 shows PLOM micrographs taken at the same T_c and time conditions for the commercial PLA and their blends with 5 wt % of *l*-PLLA and 5 wt % of *c*-PLLA, respectively.

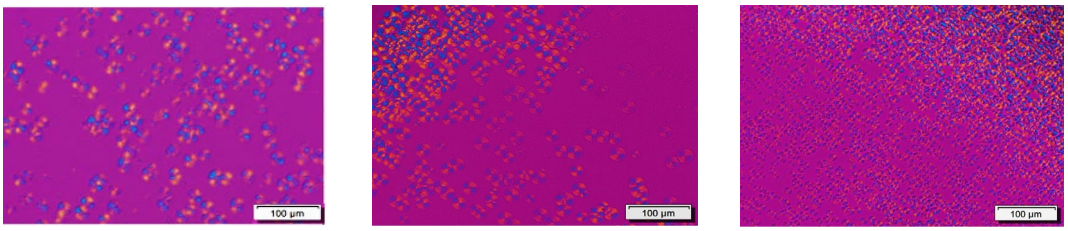

(a) PLA (b) PLA/ *l*-PLLA 95/5 (c)PLA/ *c*-PLLA 95/5

Figure 6. PLOM images taken at 115 °C, after 5 minutes, for (a) PLA, (b) PLA / *l*-PLLA 95/5, and (c) PLA / *c*-PLLA 95/5.

Figure 6 shows, qualitatively, a relatively similar nucleation density (or slightly higher) between the PLA matrix (Figure 6a) and the PLA / *l*-PLLA 95/5 blend (Figure 6b). In contrast, there is a large increase in the nucleation density of PLA when 5 wt % *c*-PLLA (Figure 6c) is

added. Once again (as in the blend with *l*-PLLA of low MW), the small amount of cyclic PLLA is acting like a nucleating agent for PLA, as *c*-PLLA can nucleate much faster than PLA, subsequently triggering its nucleation.

Spherulitic Growth rate: Plasticization-like effect and topological influence

Figure 7a shows the differences in the spherulitic growth rates for the neat components. Figure 7b shows that despite these differences, *c*-PLLA produces more significant changes when added to the PLA matrix.

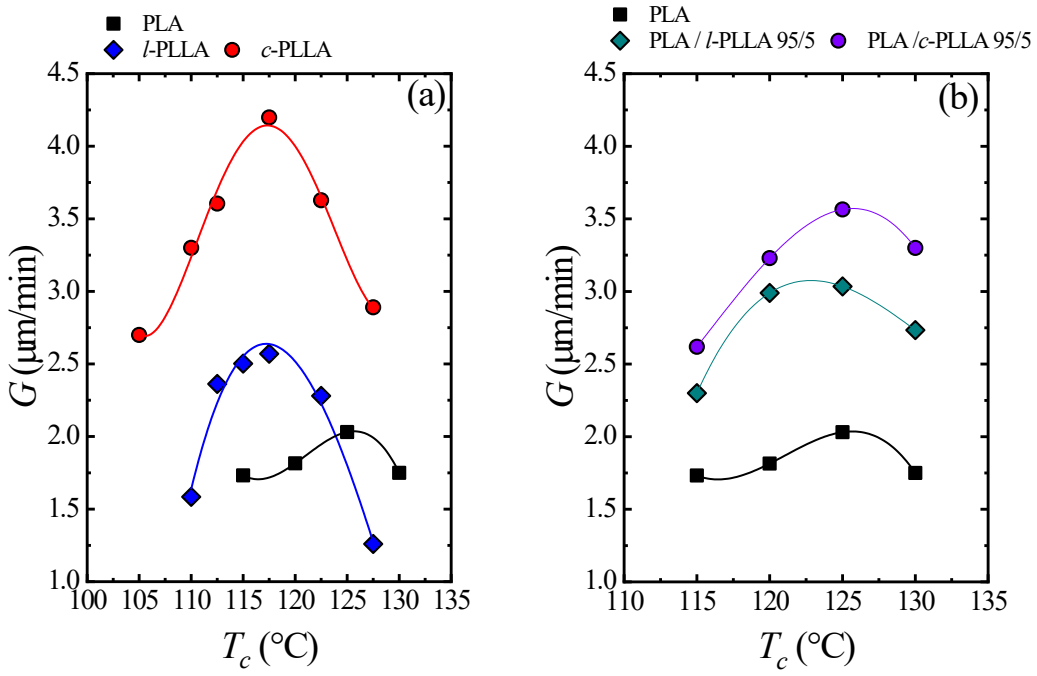

Figure 7. Spherulitic growth rate (G) as a function of the isothermal crystallization temperature (T_c) for (a) neat components, and (b) PLA and the PLA / *l*-PLLA 95/5 and PLA / *c*-PLLA 95/5 blends. The solid lines are to guide the eye.

In Figure 7a, the differences between *c*-PLLA and *l*-PLLA have already been discussed above. The lower spherulitic growth rate for PLA at temperatures below 125 ºC stems from its slower chain diffusion caused by its much higher MW. It has been reported that for linear PLA

with M_n ranging from 1 to 200 kg/mol, G increases as M_n decreases [8]. Also, due to the MW effect, the maximum in $G_{,PLA}$ occurs at higher T_c values than that for *l*-PLLA and *c*-PLLA. In the case of the blends, Figure 7b shows that both PLA / *l*-PLLA 95/5 and PLA / *c*-PLLA 95/5 blends have higher G values compared to neat PLA. As in the nucleation case (Figure 6), the 5 wt % *c*-PLLA addition has a stronger influence on neat PLA (in comparison with 5 wt % *l*-PLLA addition), causing the highest G values. Considering the similar MW between *l*-PLLA and *c*-PLLA, the enhanced nucleation and crystallization values reached by adding *c*-PLLA (in comparison with *l*-PLLA) can be attributed to its cyclic topology, a remarkable result.

3.2.2 DSC Non-isothermal experiments

Figure 8 shows the non-isothermal scans for the PLA and their blends with *l*- and *c*-PLLA.

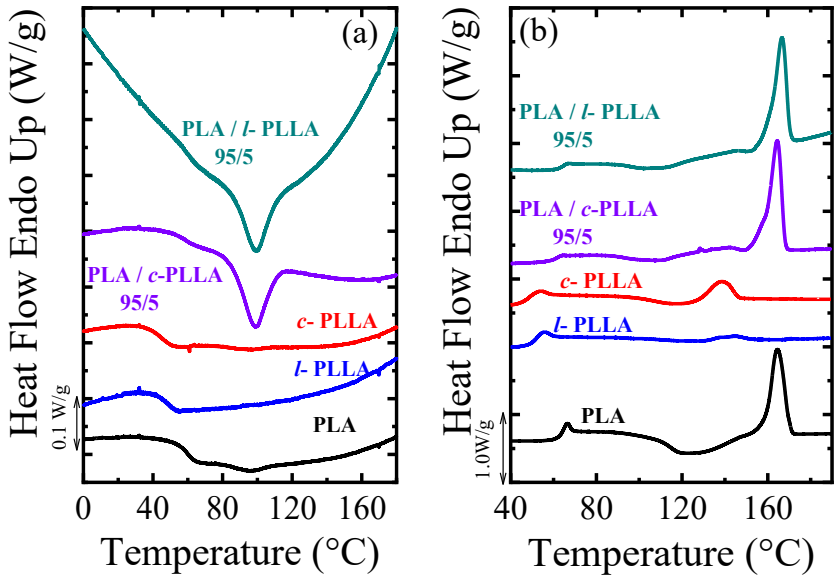

Figure 8. (a) DSC cooling scans performed at 5 °C/min, and (b) subsequent DSC heating scans at 20 °C/min for PLA and their blends with 5 wt % of *l*- or *c*-PLLA.

Figure 8a shows an exothermic peak for the PLA and their blends during cooling from the melt, at around 99 °C. The enthalpy (ΔH_c) of this peak significantly increases in the blends (see Table S3 on the SI), evidencing the enhanced crystallization process triggered by the addition of

the low MW *l*-PLLA and *c*-PLLA samples. The ΔH_c obtained for the PLA / *c*-PLLA blend is higher than that of the PLA / *l*-PLLA blend due to the topological effect.

Figure 8b shows that neither *l*-PLLA nor *c*-PLLA affect the T_m values of the PLA. The T_{cc} values of the blends are significantly lower than the $T_{cc,\ PLA}$, indicating the higher number of nuclei active in the blends, especially in the PLA / *c*-PLLA blend, that shows the lowest T_{cc} value. Also, it is observed that the addition of *c*-PLLA to neat PLA generates the lowest T_g value (note that the $T_{g,\ PLA/l\text{-}PLLA}$ is higher) compared to the PLA (see Tables S1 and S2). This indicates the higher chain mobility in this blend as a result of the plasticization-like effect.

3.2.3 Overall isothermal crystallization: Crystallization from the glassy state

Figure 9 shows a comparison of $1/\tau_0$ and $1/\tau_{50\%}$ values as a function of T_c for neat PLA, *l*-PLLA, and *c*-PLLA (Figures 9a and 9c), and a comparison of the neat PLA with the PLA / *l*-PLLA and PLA / *c*-PLLA blends (Figures 9b and 9d).

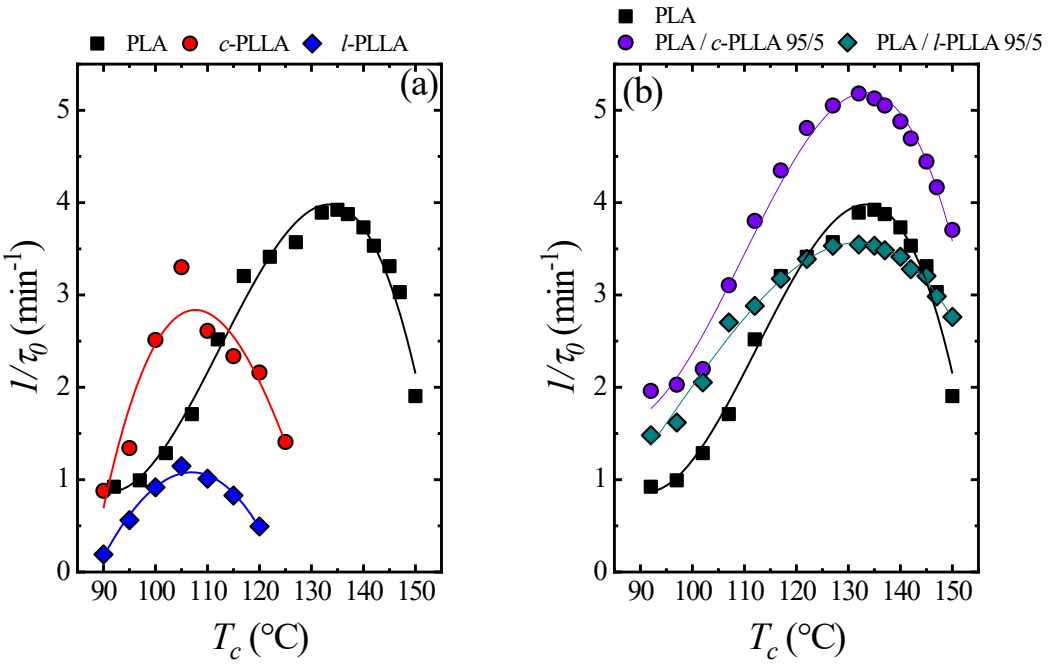

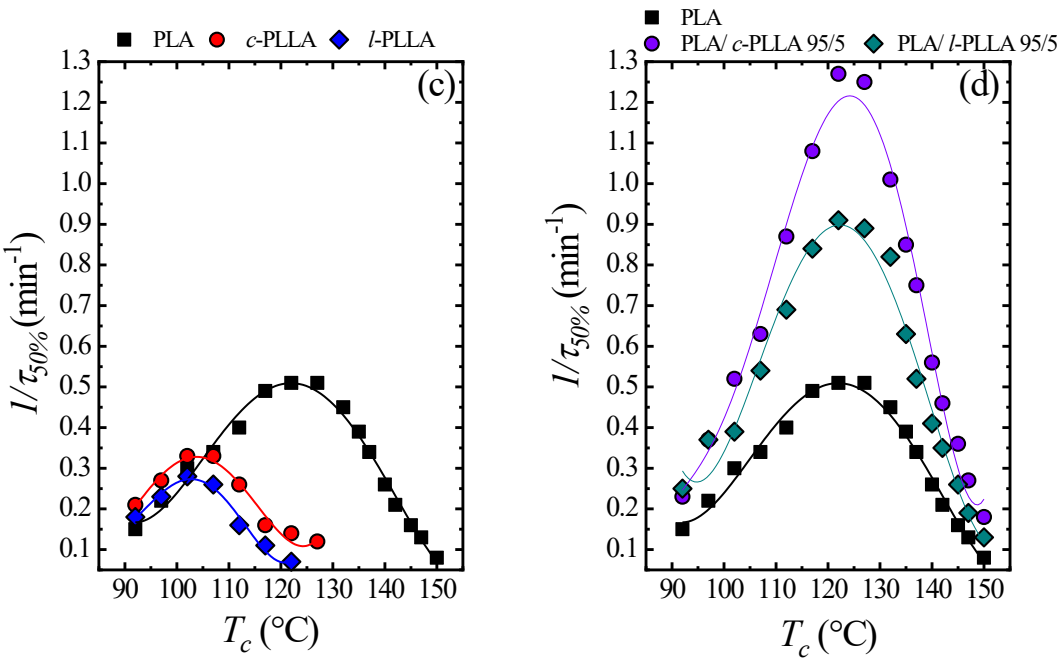

Figure 9. Inverse of the induction time ($1/\tau_0$) and inverse of half-crystallization time ($1/\tau_{50\%}$) as a function of T_c for (a) and (c) neat PLA, *l*-PLLA and *c*-PLLA; and (b) and (d) for PLA / *l*-PLLA 95/5 and PLA / *c*-PLLA 95/5 blends. The solid lines are to guide the eye.

Figures 9a and 9c show that PLA has a higher $1/\tau_0$ and $1/\tau_{50\%}$ values than low MW *l*-PLLA and *c*-PLLA. It must be remembered that in this case, the crystallization has been determined from the glassy state. Commercial high MW linear PLA (with a 2% mol of D stereoisomer) nucleates and crystallizes slowly from the melt. However, when it is crystallized from the glassy state, its nucleation density and nucleation rate are greatly enhanced. This is reflected in the high values of $1/\tau_0$ in comparison with the low MW samples (*l*-PLLA and *c*-PLLA). At a constant T_c, it is expected that the primary nucleation rate (expressed as $1/\tau_0$) increases as the MW increases [69], either at low or high T_c, whereas the $1/\tau_{50\%}$ vs. MW behavior is more complex. At low T_c, the diffusion plays a key factor, and hence the low MW chains will have a faster overall crystallization. At high T_c, the nucleation favors the high MW chains.

Figures 9a and 9c reflect that the maximum $1/\tau_0$ and $1/\tau_{50\%}$ values of the PLA occur at

higher T_c values than for *l*-PLLA and *c*-PLLA, due to the MW differences. The faster overall crystallization kinetics of the PLA is explained by the strong influence of its nucleation capacity from the glassy state. The high MW PLA has a higher nucleation density and higher nucleation rate (see Figure 9a) compared to the *l*-PLLA and *c*-PLLA. However, the *l*-PLLA and *c*-PLLA have a higher diffusion capacity due to their low MWs, and this is reflected in their higher G values, shown in Figure 7a.

Interestingly, Figure 9d shows how by adding only 5 wt % of *l*-PLLA or *c*-PLLA to the PLA matrix, a significant increase in the overall crystallization rate is obtained. Both PLA / *l*-PLLA 95/5 and PLA / *c*-PLLA 95/5 blends crystallize faster than neat PLA, even when the neat minority components were slower (see *l*-PLLA and *c*-PLLA in Figure 9c).

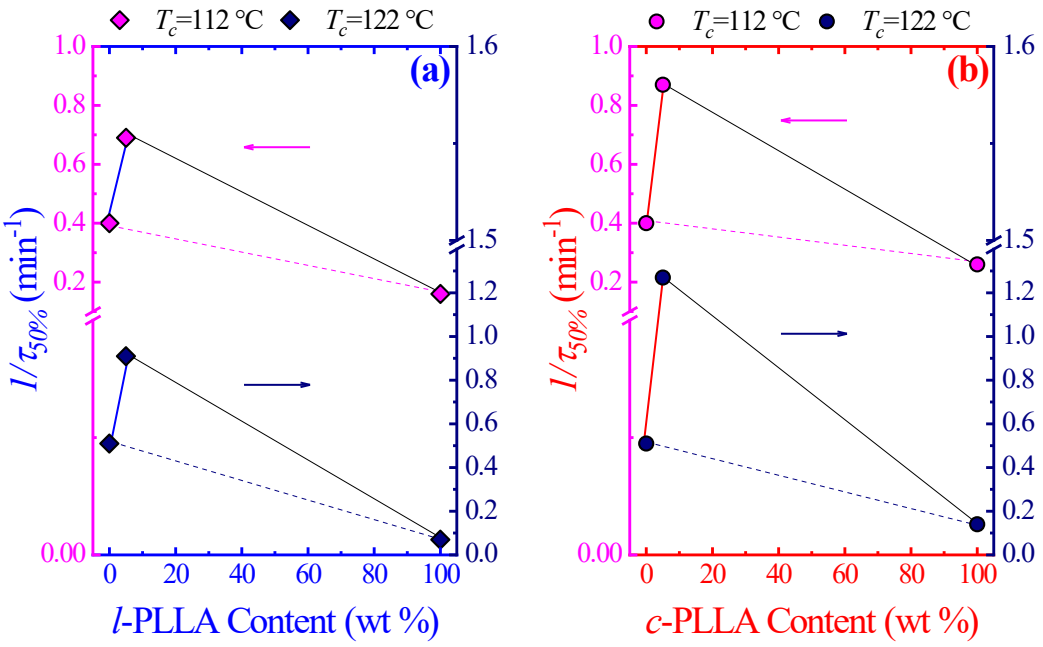

Figure 10. $1/\tau_{50\%}$ values at selected T_c=112 °C and 122 °C as a function of (a) *l*-PLLA and (b) *c*-PLLA content. The dashed line joints the *l*-PLLA and *c*-PLLA with the PLA to represent a simple mixing law, and the solid lines represent the recovery of the mixing law.

To illustrate the significant increases caused by the addition of 5 wt % of *l*-PLLA or *c*-PLLA, we have taken the $1/\tau_{50\%}$ values, at selected T_c = 112 °C and 122 °C, and plotted them as a function of the *l*-PLLA and *c*-PLLA content, for the corresponding blends, as shown in Figure 10. Figures 10a and 10b show that both *l*-PLLA and *c*-PLLA can increase $1/\tau_{50\%}$ by a factor of 1.8 and 2.5, respectively. By comparing both Figures, it is interesting to note that *c*-PLLA addition causes a higher increase than *l*-PLLA addition, independently of the selected T_c. Considering that both *l*- and *c*-PLLA have similar MWs, the higher capacity of *c*-PLLA to accelerate the overall crystallization kinetics of PLA can be attributed to a topological effect. The *l*-PLLA only acts as a plasticizer agent of the PLA since it does not affect the PLA nucleation rate (see Figure 9b), but it does affect its diffusion (see higher *G* of the PLA / *l*-PLLA blend compared to the PLA in Figure 7b). In contrast, adding *c*-PLLA to the PLA matrix has a synergistic effect since *c*-PLLA accelerates both the nucleation rate (see Figure 9b, and the higher number of nuclei in Figure 6c) and the spherulitic growth rate (see Figure 7b). Scheme 2 illustrates this situation.

Understanding the plasticization-like and synergistic effect

The main difference between linear and cyclic polymers is the lack of chain ends in the latter. This lack of chain ends causes a faster diffusion in the cyclic polymers as compared to the linear ones, as cyclic chains tend to have a significantly more compact coil conformation. If we consider a blend, the chain ends of the linear PLLA of low MW can be entangled with PLA high MW chains, as shown in the bottom part of Scheme 2a. Although the presence of these low MW linear chains improves the mobility of the high MW chains, such mobility is lower in comparison with the one caused by the cyclic chains (see Scheme 2b).

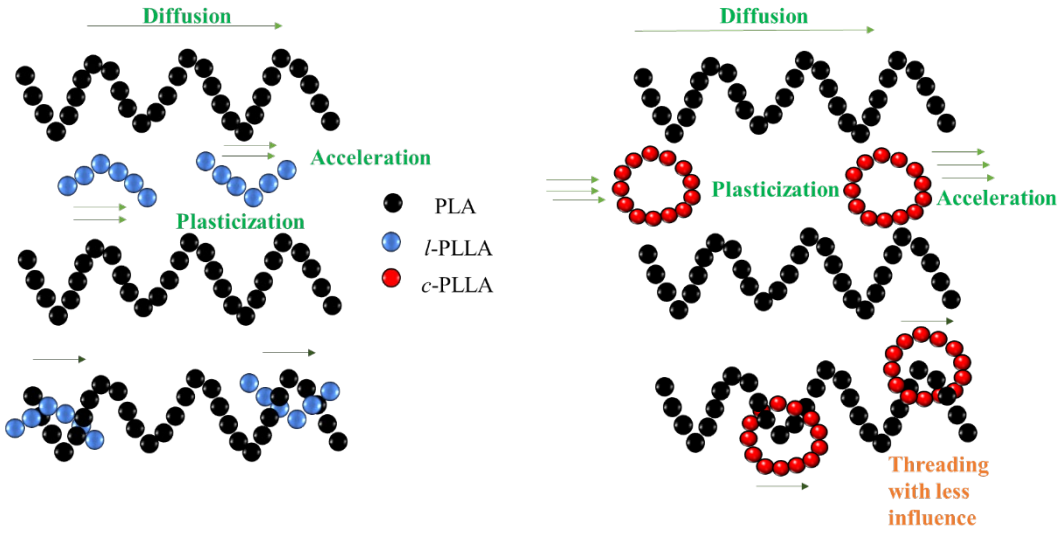

(a) PLA / *l*-PLLA 95/5 (b) PLA / *c*-PLLA 95/5

Scheme 2. Illustration of the plasticization effect induces by (a) linear chains in PLA / *l*-PLLA 95/5, and (b) cyclic chains in PLA / *c*-PLLA 95/5 blends.

When we have cyclic chains, their lack of chains ends endows them with more compact coil conformations that enhance their diffusion and make them more effective plasticizers, even if some threading effects could exist between cyclic and linear chains. Our results are in agreement with recent molecular dynamics simulations performed by Tsalikis and Mavarantzas [50]. They simulated PEO blends of linear and cyclic chains. They found that short rings were less susceptible to threading by much longer linear chains, and therefore can preserve their highly compact conformations with much faster diffusion than comparable size linear chains.

LH theory: Plasticization-like vs. Synergistics effect

As in the previous section, we applied the LH theory to the experimental data of Figure 9. We employed the $T_m°$ obtained by the HW extrapolation, in which values around 217 °C were obtained (see Table S5), in line with the values reported in the literature [20]. The K_g^{τ} values for the neat PLA and its blends are plotted in Figure 11.

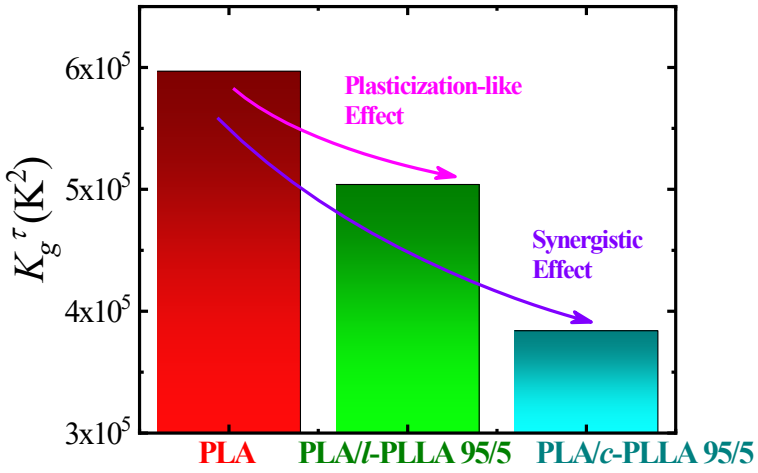

Figure 11. K_g^{τ} for the PLA and the PLA / *l*-PLLA 95/5 and PLA / *c*-PLLA 95/5 blends. The curve lines indicate the different effect of *l*-PLLA (plasticization-like) and *c*-PLLA (synergistic) in the PLA matrix.

Figure 11 shows the reduction of the K_g^{τ} value of the PLA compared with its blends indicating that either *l*-PLLA and *c*-PLLA facilitates the crystallization of the PLA (a similar trend is obtained for the K_g^{G} values in Table S7). The lower K_g^{τ}, $_{c\text{-}PLLA}$ compared to K_g^{τ}, $_{l\text{-}PLLA}$ suggests the influence of the topology (note that *l*- and *c*-PLLA have a similar MW and the same content in the blend). The *c*-PLLA provokes higher nucleation and higher diffusion of the PLA matrix chains, thereby accelerating $1/\tau_0$, G, and $1/\tau_{50\%}$ values.

4. Conclusions

Linear and cyclic low MW PLLAs were blended with small amounts of their counterparts. For the *l*-PLLA rich blends, it was found for the first time that small amounts of *c*-PLLA cause a synergistic effect (*i.e.*, nucleation plus plasticization effects) since the nucleation density, nucleation rate ($1/\tau_0$), spherulitic growth rates (G), and overall crystallization rates ($1/\tau_{50\%}$) increase compared to the values obtained for neat *l*-PLLA. These effects were found to be higher when the

c-PLLA content increased from 5 to 10 wt %. In contrast, in the *c*-PLLA rich blends, adding small amounts of *l*-PLLA caused opposite effects: reductions in nucleation density, $1/\tau_0$, G, and $1/\tau_{50\%}$ values, due to threading of the linear chains through the cyclic ones.

Low MW *l*-PLLA and *c*-PLLA in small amounts were blended, for the first time, with a commercial high MW PLA, causing different effects, depending on the topology (*i.e.*, linear vs. cyclic) on the spherulitic growth rate, nucleation rate, and overall crystallization kinetics without depressing the melting temperatures. The *l*-PLLA acts only as a plasticizer of the PLA matrix, as expected, accelerating its spherulitic growth rate but without affecting the nucleation density or the nucleation rate. In contrast, the *c*-PLLA has a remarkable synergistic effect on the high MW PLA matrix. The *c*-PLLA not only accelerates the spherulitic growth rate but also the nucleation rate, and hence the overall crystallization rate of the PLA matrix. These rate enhancements on the PLA matrix caused by adding *c*-PLLA, reported also for the first time, are explained by the unique topology of cyclic polymers.

ACKNOWLEDGMENTS

We would like to acknowledge the financial support from the BIODEST project; this project has received funding from the European Union's Horizon 2020 research and innovation programme under the Marie Skłodowska-Curie grant agreement No 778092. This work has also received funding from the Basque Government through grant IT1309-19. R.A.P.-C is supported by PIFI of the Chinese Academy of Science for international postdoctoral researchers (2019PE0004), the China Postdoctoral Science Foundation (2020M670462), and National Natural Science Foundation of China (NSFC) (52050410327) under the program Research Fund for International Young Scientists. O.C. is Senior Research Associate for the F.R.S.-FNRS of Belgium.

Supporting Information

Additional DSC curves and data Tables and Hoffman-Weeks extrapolations are included. Data pertaining the application of the Avrami and Lauritzen and Hoffman crystallization theories (using the Crystallization Fit App, see ref. [66]) are also included.

5. References

[1] E. Louisy, G. Fontaine, V. Gaucher, F. Bonnet, G. Stoclet, Comparative studies of thermal and mechanical properties of macrocyclic versus linear polylactide, Polymer Bulletin (2020).
[2] L. Avérous, Chapter 21 - Polylactic Acid: Synthesis, Properties and Applications, in: M.N. Belgacem, A. Gandini (Eds.), Monomers, Polymers and Composites from Renewable Resources, Elsevier, Amsterdam, 2008, pp. 433-450.
[3] S. Saeidlou, M.A. Huneault, H. Li, C.B. Park, Poly(lactic acid) crystallization, Progress in Polymer Science 37(12) (2012) 1657-1677.
[4] H. Li, M.A. Huneault, Effect of nucleation and plasticization on the crystallization of poly(lactic acid), Polymer 48(23) (2007) 6855-6866.
[5] J.-M. Raquez, Y. Habibi, M. Murariu, P. Dubois, Polylactide (PLA)-based nanocomposites, Progress in Polymer Science 38(10) (2013) 1504-1542.
[6] D.Y. Kim, J.B. Lee, D.Y. Lee, K.H. Seo, Plasticization Effect of Poly(Lactic Acid) in the Poly(Butylene Adipate–co–Terephthalate) Blown Film for Tear Resistance Improvement, Polymers 12(9) (2020) 1904.
[7] O. Martin, L. Avérous, Poly(lactic acid): plasticization and properties of biodegradable multiphase systems, Polymer 42(14) (2001) 6209-6219.
[8] A.J. Müller, M. Ávila, G. Saenz, J. Salazar, CHAPTER 3 Crystallization of PLA-based Materials, Poly(lactic acid) Science and Technology: Processing, Properties, Additives and Applications, The Royal Society of Chemistry2015, pp. 66-98.
[9] B. Brüster, A. Montesinos, P. Reumaux, R.A. Pérez-Camargo, A. Mugica, M. Zubitur, A.J. Müller, P. Dubois, F. Addiego, Crystallization kinetics of polylactide: Reactive plasticization and reprocessing effects, Polymer Degradation and Stability 148 (2018) 56-66.
[10] L. Jiang, T. Shen, P. Xu, X. Zhao, X. Li, W. Dong, P. Ma, M. Chen, Crystallization modification of poly(lactide) by using nucleating agents and stereocomplexation, e-Polymers 16(1) (2016) 1.
[11] H. Tsuji, H. Takai, N. Fukuda, H. Takikawa, Non-Isothermal Crystallization Behavior of Poly(L-lactic acid) in the Presence of Various Additives, Macromolecular Materials and Engineering 291(4) (2006) 325-335.
[12] J.Y. Nam, S. Sinha Ray, M. Okamoto, Crystallization Behavior and Morphology of Biodegradable Polylactide/Layered Silicate Nanocomposite, Macromolecules 36(19) (2003) 7126-7131.
[13] A. Kovalcik, R.A. Pérez-Camargo, C. Fürst, P. Kucharczyk, A.J. Müller, Nucleating efficiency and thermal stability of industrial non-purified lignins and ultrafine talc in poly(lactic acid) (PLA), Polymer Degradation and Stability 142 (2017) 244-254.

[14] L. He, F. Song, D.-F. Li, X. Zhao, X.-L. Wang, Y.-Z. Wang, Strong and Tough Polylactic Acid Based Composites Enabled by Simultaneous Reinforcement and Interfacial Compatibilization of Microfibrillated Cellulose, ACS Sustainable Chemistry & Engineering 8(3) (2020) 1573-1582.
[15] K.S. Anderson, M.A. Hillmyer, Melt preparation and nucleation efficiency of polylactide stereocomplex crystallites, Polymer 47(6) (2006) 2030-2035.
[16] S.C. Schmidt, M.A. Hillmyer, Polylactide stereocomplex crystallites as nucleating agents for isotactic polylactide, Journal of Polymer Science Part B: Polymer Physics 39(3) (2001) 300-313.
[17] H. Tsuji, Poly(lactic acid) stereocomplexes: A decade of progress, Advanced Drug Delivery Reviews 107 (2016) 97-135.
[18] M. Nofar, D. Sacligil, P.J. Carreau, M.R. Kamal, M.-C. Heuzey, Poly (lactic acid) blends: Processing, properties and applications, International Journal of Biological Macromolecules 125 (2019) 307-360.
[19] G. Giacobazzi, M. Rizzuto, M. Zubitur, A. Mugica, D. Caretti, A.J. Müller, Crystallization kinetics as a sensitive tool to detect degradation in poly(lactide)/poly(ε-caprolactone)/ PCL-co-PC copolymers blends, Polymer Degradation and Stability 168 (2019) 108939.
[20] M.L. Di Lorenzo, R. Androsch, Accelerated crystallization of high molar mass poly(l/d-lactic acid) by blending with low molar mass poly(l-lactic acid), European Polymer Journal 100 (2018) 172-177.
[21] F.M. Haque, S.M. Grayson, The synthesis, properties and potential applications of cyclic polymers, Nature Chemistry 12(5) (2020) 433-444.
[22] R. Liénard, J. De Winter, O. Coulembier, Cyclic polymers: Advances in their synthesis, properties, and biomedical applications, Journal of Polymer Science 58(11) (2020) 1481-1502.
[23] Y. Tezuka, Cyclic and topological polymers: Ongoing innovations and upcoming breakthroughs, Reactive and Functional Polymers 148 (2020) 104489.
[24] B. Golba, E.M. Benetti, B.G. De Geest, Biomaterials applications of cyclic polymers, Biomaterials (2020) 120468.
[25] R.A. Pérez, M.E. Córdova, J.V. López, J.N. Hoskins, B. Zhang, S.M. Grayson, A.J. Müller, Nucleation, crystallization, self-nucleation and thermal fractionation of cyclic and linear poly(ε-caprolactone)s, Reactive and Functional Polymers 80 (2014) 71-82.
[26] R.A. Pérez-Camargo, A. Mugica, M. Zubitur, A.J. Müller, Crystallization of Cyclic Polymers, in: F. Auriemma, G.C. Alfonso, C. de Rosa (Eds.), Polymer Crystallization I: From Chain Microstructure to Processing, Springer International Publishing, Cham, 2017, pp. 93-132.
[27] N. Zaldua, R. Liénard, T. Josse, M. Zubitur, A. Mugica, A. Iturrospe, A. Arbe, J. De Winter, O. Coulembier, A.J. Müller, Influence of Chain Topology (Cyclic versus Linear) on the Nucleation and Isothermal Crystallization of Poly(l-lactide) and Poly(d-lactide), Macromolecules 51(5) (2018) 1718-1732.
[28] Y. Tezuka, T. Ohtsuka, K. Adachi, R. Komiya, N. Ohno, N. Okui, A Defect-Free Ring Polymer: Size-Controlled Cyclic Poly(tetrahydrofuran) Consisting Exclusively of the Monomer Unit, Macromolecular Rapid Communications 29(14) (2008) 1237-1241.
[29] T. Kitahara, S. Yamazaki, K. Kimura, Effects of Topological Constraint and Knot Entanglement on the Crystal Growth of Polymers Proved by Growth Rate of Spherulite of Cyclic Polyethylene, KOBUNSHI RONBUNSHU 68(10) (2011) 694-701.
[30] S. Nam, J. Leisen, V. Breedveld, H.W. Beckham, Dynamics of unentangled cyclic and linear poly(oxyethylene) melts, Polymer 49(25) (2008) 5467-5473.
[31] J. Cooke, K. Viras, G.-E. Yu, T. Sun, T. Yonemitsu, A.J. Ryan, C. Price, C. Booth, Large

Cyclic Poly(oxyethylene)s: Chain Folding in the Crystalline State Studied by Raman Spectroscopy, X-ray Scattering, and Differential Scanning Calorimetry, Macromolecules 31(9) (1998) 3030-3039.
[32] G.-E. Yu, T. Sun, Z.-G. Yan, C. Price, C. Booth, J. Cook, A.J. Ryan, K. Viras, Low-molar-mass cyclic poly(oxyethylene)s studied by Raman spectroscopy, X-ray scattering and differential scanning calorimetry, Polymer 38(1) (1997) 35-42.
[33] G. Zardalidis, J. Mars, J. Allgaier, M. Mezger, D. Richter, G. Floudas, Influence of chain topology on polymer crystallization: poly(ethylene oxide) (PEO) rings vs. linear chains, Soft Matter 12(39) (2016) 8124-8134.
[34] H.-H. Su, H.-L. Chen, A. Díaz, M.T. Casas, J. Puiggalí, J.N. Hoskins, S.M. Grayson, R.A. Pérez, A.J. Müller, New insights on the crystallization and melting of cyclic PCL chains on the basis of a modified Thomson–Gibbs equation, Polymer 54(2) (2013) 846-859.
[35] R.A. Pérez, J.V. López, J.N. Hoskins, B. Zhang, S.M. Grayson, M.T. Casas, J. Puiggalí, A.J. Müller, Nucleation and Antinucleation Effects of Functionalized Carbon Nanotubes on Cyclic and Linear Poly(ε-caprolactones), Macromolecules 47(11) (2014) 3553-3566.
[36] J.V. López, R.A. Pérez-Camargo, B. Zhang, S.M. Grayson, A.J. Müller, The influence of small amounts of linear polycaprolactone chains on the crystallization of cyclic analogue molecules, RSC Advances 6(53) (2016) 48049-48063.
[37] K. Schäler, E. Ostas, K. Schröter, T. Thurn-Albrecht, W.H. Binder, K. Saalwächter, Influence of Chain Topology on Polymer Dynamics and Crystallization. Investigation of Linear and Cyclic Poly(ε-caprolactone)s by 1H Solid-State NMR Methods, Macromolecules 44(8) (2011) 2743-2754.
[38] K.S. Lee, G. Wegner, Linear and cyclic alkanes (CnH2n+2, CNH2n) with n > 100. Synthesis and evidence for chain-folding, Die Makromolekulare Chemie, Rapid Communications 6(3) (1985) 203-208.
[39] C.W. Bielawski, D. Benitez, R.H. Grubbs, An "Endless" Route to Cyclic Polymers, Science 297(5589) (2002) 2041-2044.
[40] M.E. Córdova, A.T. Lorenzo, A.J. Müller, J.N. Hoskins, S.M. Grayson, A Comparative Study on the Crystallization Behavior of Analogous Linear and Cyclic Poly(ε-caprolactones), Macromolecules 44(7) (2011) 1742-1746.
[41] E.J. Shin, W. Jeong, H.A. Brown, B.J. Koo, J.L. Hedrick, R.M. Waymouth, Crystallization of Cyclic Polymers: Synthesis and Crystallization Behavior of High Molecular Weight Cyclic Poly(ε-caprolactone)s, Macromolecules 44(8) (2011) 2773-2779.
[42] W. Ryu, L. Xiang, T. Jeon, M. Ree, Melt density, equilibrium melting temperature, and crystallization characteristics of highly pure cyclic poly(ε-Caprolactone)s, Polymer 207 (2020) 122899.
[43] H. Takeshita, M. Poovarodom, T. Kiya, F. Arai, K. Takenaka, M. Miya, T. Shiomi, Crystallization behavior and chain folding manner of cyclic, star and linear poly(tetrahydrofuran)s, Polymer 53(23) (2012) 5375-5384.
[44] R. Ono, H. Atarashi, S. Yamazaki, K. Kimura, Molecular weight dependence of the growth rate of spherulite of cyclic poly(ε-caprolactone) polymerized by ring expansion reaction, Polymer 194 (2020) 122403.
[45] K. Iyer, M. Muthukumar, Langevin dynamics simulation of crystallization of ring polymers, 148(24) (2018) 244904.
[46] H. Xiao, C. Luo, D. Yan, J.-U. Sommer, Molecular Dynamics Simulation of Crystallization Cyclic Polymer Melts As Compared to Their Linear Counterparts, Macromolecules 50(24) (2017) 9796-9806.

[47] R.-J. Liu, Z.-P. Zhou, Y. Liu, Z.-P. Liang, Y.-Q. Ming, T.-F. Hao, Y.-J. Nie, Differences in Crystallization Behaviors between Cyclic and Linear Polymer Nanocomposites, Chinese Journal of Polymer Science 38(9) (2020) 1034-1044.
[48] G. Subramanian, S. Shanbhag, Conformational properties of blends of cyclic and linear polymer melts, Phys Rev E Stat Nonlin Soft Matter Phys 77(1 Pt 1) (2008) 14.
[49] G. Subramanian, A topology preserving method for generating equilibrated polymer melts in computer simulations, Journal of Chemical Physics 133 (2010) 164902.
[50] D.G. Tsalikis, V.G. Mavrantzas, Size and Diffusivity of Polymer Rings in Linear Polymer Matrices: The Key Role of Threading Events, Macromolecules 53(3) (2020) 803-820.
[51] D.G. Tsalikis, V.G. Mavrantzas, Threading of Ring Poly(ethylene oxide) Molecules by Linear Chains in the Melt, ACS Macro Letters 3(8) (2014) 763-766.
[52] W. Wang, C.S. Biswas, C. Huang, H. Zhang, C.-Y. Liu, F.J. Stadler, B. Du, Z.-C. Yan, Topological Effect on Effective Local Concentration and Dynamics in Linear/Linear, Ring/Ring, and Linear/Ring Miscible Polymer Blends, Macromolecules 53(2) (2020) 658-668.
[53] G. Subramanian, S. Shanbhag, Self-Diffusion in Binary Blends of Cyclic and Linear Polymers, Macromolecules 41(19) (2008) 7239-7242.
[54] G. Subramanian, S. Shanbhag, Conformational free energy of melts of ring-linear polymer blends, Phys Rev E Stat Nonlin Soft Matter Phys 80(4 Pt 1) (2009) 21.
[55] M. Kruteva, J. Allgaier, D. Richter, Direct Observation of Two Distinct Diffusive Modes for Polymer Rings in Linear Polymer Matrices by Pulsed Field Gradient (PFG) NMR, Macromolecules 50(23) (2017) 9482-9493.
[56] E.J. Shin, A.E. Jones, R.M. Waymouth, Stereocomplexation in Cyclic and Linear Polylactide Blends, Macromolecules 45(1) (2012) 595-598.
[57] M. Kapnistos, M. Lang, D. Vlassopoulos, W. Pyckhout-Hintzen, D. Richter, D. Cho, T. Chang, M. Rubinstein, Unexpected power-law stress relaxation of entangled ring polymers, Nature Materials 7(12) (2008) 997-1002.
[58] O. Coulembier, P. Dubois, 4-dimethylaminopyridine-based organoactivation: From simple esterification to lactide ring-opening "Living" polymerization, 50(9) (2012) 1672-1680.
[59] O. Coulembier, J. De Winter, T. Josse, L. Mespouille, P. Gerbaux, P. Dubois, One-step synthesis of polylactide macrocycles from sparteine-initiated ROP, Polymer Chemistry 5(6) (2014) 2103-2108.
[60] D. Turnbull, J.C. Fisher, Rate of Nucleation in Condensed Systems, 17(1) (1949) 71-73.
[61] R. Becker, W. Döring, Kinetische Behandlung der Keimbildung in übersättigten Dämpfen, 416(8) (1935) 719-752.
[62] A.T. Lorenzo, M.L. Arnal, J. Albuerne, A.J. Müller, DSC isothermal polymer crystallization kinetics measurements and the use of the Avrami equation to fit the data: Guidelines to avoid common problems, Polymer Testing 26(2) (2007) 222-231.
[63] M. Avrami, Granulation, Phase Change, and Microstructure Kinetics of Phase Change. III, The Journal of Chemical Physics 9(2) (1941) 177-184.
[64] J.I. Lauritzen, J.D. Hoffman, Theory of Formation of Polymer Crystals with Folded Chains in Dilute Solution, J. Res. Natl. Bur. Stand., Sect. A 64A(1) (1960) 73-102.
[65] J.D. Hoffman, J.I. Lauritzen, Crystallization of Bulk Polymers With Chain Folding: Theory of Growth of Lamellar Spherulites J. Res. Natl. Bur. Stand., Sect. A 65A(4) (1961) 297-336.
[66] OriginLab, Crystallization Fit, 2021. https://www.originlab.com/fileExchange/details.aspx?fid=597. (Accessed March 09, 2021 2021).
[67] A.T. Lorenzo, A.J. Müller, Estimation of the nucleation and crystal growth contributions to

the overall crystallization energy barrier, Journal of Polymer Science Part B: Polymer Physics 46(14) (2008) 1478-1487.
[68] A.J. Müller, R.M. Michell, A.T. Lorenzo, Isothermal Crystallization Kinetics of Polymers, Polymer Morphology2016, pp. 181-203.
[69] N. Okui, S. Umemoto, R. Kawano, A. Mamun, Temperature and Molecular Weight Dependencies of Polymer Crystallization, in: G. Reiter, G.R. Strobl (Eds.), Progress in Understanding of Polymer Crystallization, Springer Berlin Heidelberg, Berlin, Heidelberg, 2007, pp. 391-425.